

Quantum filaments in dipolar Bose-Einstein condensates

F. Wächtler and L. Santos

Institut für Theoretische Physik, Leibniz Universität Hannover, Appelstrasse 2, DE-30167 Hannover, Germany

(Received 26 January 2016; published 24 June 2016)

Collapse in dipolar Bose-Einstein condensates may be arrested by quantum fluctuations. Due to the anisotropy of the dipole-dipole interactions, the dipole-driven collapse induced by soft excitations is compensated by the repulsive Lee-Huang-Yang contribution resulting from quantum fluctuations of hard excitations, in a similar mechanism as that recently proposed for Bose-Bose mixtures. The arrested collapse results in self-bound filamentlike droplets, providing an explanation for the intriguing results of recent dysprosium experiments. Arrested instability and droplet formation are general features directly linked to the nature of the dipole-dipole interactions, and should hence play an important role in all future experiments with strongly dipolar gases.

DOI: [10.1103/PhysRevA.93.061603](https://doi.org/10.1103/PhysRevA.93.061603)

Dipole-dipole interactions (DDIs) lead to qualitatively new physics for dipolar gases compared to nondipolar ones [1,2]. As a result, this physics constitutes the focus of a large interest, including experiments on magnetic atoms [3–6], polar molecules [7–10], and Rydberg-dressed atoms [11]. A characteristic feature of dipolar Bose-Einstein condensates (BECs) is their geometry-dependent stability [12]. If the condensate is elongated along the dipole orientation, the DDIs are attractive in average, and the BEC may become unstable. Chromium experiments showed that, as for the case of a nondipolar BEC with negative s -wave scattering length, $a < 0$, the unstable BEC collapses, albeit with a peculiar d -wave postcollapse dynamics [13].

This picture has been challenged by recent dysprosium (Dy) experiments [14], in which destabilization, induced by a quench to a sufficiently low a , is not followed by collapse, but rather by the formation of stable droplets that are only destroyed in a long-time scale by weak three-body losses (3BLs). This surprising result, which resembles the Rosensweig instability in ferrofluids [15,16], points to an up to now unknown stabilization mechanism that plays a similar role as that of surface tension in classical ferrofluids. It has been recently suggested that large conservative three-body forces, with a strength several orders of magnitude larger than the 3BLs, may account for the observation [17,18]. There is, however, no justification of why large three-body forces should be present, or whether there is a link between them and the DDIs.

This Rapid Communication shows that quantum fluctuations, as suggested by very recent experiments [19], provide a mechanism that accounts for the droplet stability. As recently shown [20], Lee-Huang-Yang (LHY) corrections may stabilize droplets in unstable Bose-Bose mixtures. This effect results from the presence of soft and hard elementary excitations. Whereas soft modes may become unstable, quantum fluctuations of the hard modes balance the instability, resulting in an equilibrium droplet. As shown below, due to the anisotropy of the DDIs, a dipolar BEC also presents soft and hard modes, characterized in free space by momenta perpendicular or parallel to the dipole orientation. Quantum fluctuations of hard modes provide an effective repulsion that arrest local collapses at large-enough densities, resulting in droplet nucleation (Fig. 1). We show by means of a generalized nonlocal nonlinear

Schrödinger equation (NLNLSE) that this mechanism explains the Dy results. We stress that LHY stabilization and droplet formation result from the peculiar nature of the DDIs, being characteristic features of strongly dipolar gases that should play an important role in future experiments.

We consider a BEC of magnetic dipoles of mass m and dipole moment μ oriented along the z direction by an external magnetic field (equivalent results can be found for electric dipoles). In mean field (MF), the physics is given by the NLNLSE [1],

$$i\hbar\dot{\psi}(\mathbf{r}) = \left[\frac{-\hbar^2\nabla^2}{2m} + V(\mathbf{r}) + g|\psi(\mathbf{r})|^2 + \Phi(\mathbf{r}) \right] \psi(\mathbf{r}), \quad (1)$$

with $\psi(\mathbf{r})$ the BEC wave function, $V(\mathbf{r})$ the trapping potential, $g = \frac{4\pi\hbar^2 a}{m}$, and $\Phi(\mathbf{r}) = \int d^3r' V_{dd}(\mathbf{r} - \mathbf{r}') |\psi(\mathbf{r}')|^2$, with $V_{dd}(\mathbf{r}) = \frac{\mu_0|\mu|^2}{4\pi r^3} (1 - 3\cos^2\theta)$, where μ_0 is the vacuum permittivity, and θ is the angle between \mathbf{r} and μ .

In the homogeneous case, $V(\mathbf{r}) = 0$ with density n , elementary excitations with momentum \mathbf{k} have an energy $E(\mathbf{k}) = \sqrt{\epsilon_k[\epsilon_k + 2gnf(\epsilon_{dd}, \theta_k)]}$, where $\epsilon_k = \frac{\hbar^2 k^2}{2m}$, and $f(\epsilon_{dd}, \theta_k) = 1 + \epsilon_{dd}(3\cos^2\theta_k - 1)$, with $\epsilon_{dd} = \frac{\mu_0|\mu|^2}{3g}$, and θ_k the angle between \mathbf{k} and μ . Due to the anisotropy of the DDIs, excitations with $\cos^2\theta_k > 1/3$ ($< 1/3$) become harder (softer) with growing ϵ_{dd} . For $\epsilon_{dd} > 1$, long-wavelength excitations with $\theta_k = \pi/2$ drive the BEC unstable. Quantum fluctuations of the excitations result in the LHY correction of the chemical potential [21–23],

$$\Delta\mu(n, \epsilon_{dd}) = \frac{32}{3\sqrt{\pi}} gn\sqrt{na^3} F(\epsilon_{dd}), \quad (2)$$

with $F(\epsilon_{dd}) = \frac{1}{2} \int d\theta_k \sin\theta_k f(\epsilon_{dd}, \theta_k)^{5/2}$. In the vicinity of the instability, $\epsilon_{dd} \sim 1$, the overwhelming contribution to $F(\epsilon_{dd})$ stems from hard modes. Crucially, this is true even when the BEC becomes unstable. This situation, with unstable soft modes and LHY correction dominated by stable hard modes, resembles the recently discussed case of Bose-Bose mixtures [20]. As for that scenario, the contribution of the unstable modes is negligible for $\epsilon_{dd} \sim 1$, and quantum fluctuations of the hard modes result in a repulsive LHY correction $\propto n^{3/2}$.

Let us consider at this point a harmonically trapped BEC, $V(\mathbf{r}) = \frac{1}{2}m(\omega_x^2 x^2 + \omega_y^2 y^2 + \omega_z^2 z^2)$. The treatment of

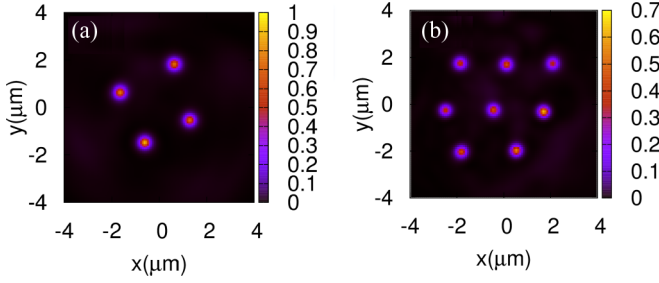


FIG. 1. Crystal-like droplet arrangements of $n_{xy}(x,y)/N$, with $n_{xy}(x,y) = \int dz n(\mathbf{r})$, for a BEC of (a) $N = 7500$ atoms and (b) 15 000 atoms, initially formed with $a = 120a_B$, 20 ms after a quench to $a = 70a_B$.

beyond MF corrections is in general involved. In the Thomas-Fermi (TF) regime one may evaluate the effect of quantum fluctuations by treating the excitations quasiclassically and employing local density approximation (LDA), obtaining a corrected equation of state [22,23], $\mu[n(\mathbf{r})] = V(\mathbf{r}) + \mu_0[n(\mathbf{r}),\epsilon_{dd}] + \Delta\mu[n(\mathbf{r}),\epsilon_{dd}]$, with $\mu_0[n(\mathbf{r}),\epsilon_{dd}] = gn(\mathbf{r}) + \int d^3r' V_{dd}(\mathbf{r} - \mathbf{r}')n(\mathbf{r}')$. One may then insert this correction in a generalized NLNLSE,

$$i\hbar\dot{\psi}(\mathbf{r}) = [\hat{H}_0 + \mu_0[n(\mathbf{r}),\epsilon_{dd}] + \Delta\mu[n(\mathbf{r}),\epsilon_{dd}]]\psi(\mathbf{r}), \quad (3)$$

with $\hat{H}_0 \equiv \frac{-\hbar^2\nabla^2}{2m} + V(\mathbf{r})$. This equation is appealing since it allows for a simplified analysis of the effects of quantum fluctuations in the TF regime. Our simulations below are performed using the split operator technique, and treating the DDIs using convolution theorem and fast-Fourier transformation. Following Ref. [24], we employ a cutoff of the DDIs to reduce spurious boundary effects.

The use of the LDA must be carefully considered. All droplets discussed below are in the TF regime along z , whereas only large droplets are in the TF regime also along xy . For small droplets, with less than 4000 atoms, the xy density profile approaches rather a Gaussian form. One may, however, show that the LHY correction is dominated by excitations with a wavelength much smaller than the droplet size. We consider a low-momentum cutoff $q_c(\theta) = q_z(\cos^2\theta + \lambda^2\sin^2\theta)^{1/2}$, with λ the aspect ratio of the droplet, and q_z the cutoff along z . Introducing this cutoff in the LHY calculation for a homogeneous space with density n results in a modified correction

$$\frac{\Delta\mu_c}{\Delta\mu} = \frac{15\sqrt{2}}{16} \frac{\int_0^\pi d\theta \sin\theta \chi(\epsilon_{dd},\theta)}{\int_0^\pi d\theta \sin\theta f(\epsilon_{dd},\theta)^{5/2}}, \quad (4)$$

where

$$\begin{aligned} \chi(\epsilon_{dd},\theta) &= 2^{5/2} \left(\frac{2f(\epsilon_{dd},\theta)}{15} - \frac{q_c(\theta)^2}{2} \right) \left(\frac{q_c(\theta)^2}{2} + f(\epsilon_{dd},\theta) \right)^{3/2} \\ &+ \frac{q_c(\theta)^5}{5} + \frac{q_c(\theta)^3}{3} f(\epsilon_{dd},\theta) - \frac{q_c(\theta)}{2} f(\epsilon_{dd},\theta)^2, \end{aligned} \quad (5)$$

and $q_c(\theta)$ is in units of ξ^{-1} , with $\xi = (8\pi na)^{-1/2}$. In the calculations discussed below, a droplet with 1000 particles has for $a = 70a_B$ a z size of $\simeq 2 \mu\text{m} \simeq 25\xi$ (with ξ calculated for an averaged central density of $1.5 \times 10^{21} \text{ m}^{-3}$), and an

aspect ratio $\lambda \simeq 6$. For a z cutoff $q_z\xi \simeq 0.25$, excitations with $|\mathbf{q}(\theta)| > q_c(\theta)$ may be considered as having a wavelength much smaller than the droplet size. For this cutoff, we obtain $\frac{\Delta\mu_c}{\Delta\mu} \simeq 0.8$, showing a large contribution of short-wavelength excitations to the LHY correction. The correction due to long-wavelength modes may modify the prefactor of the LHY correction, but the bulk of the effect is well recovered by Eq. (3). We postpone for a future analysis the detailed study of the effect of long-wavelength excitations. In addition, the validity of Eq. (3) demands a small quantum depletion [21–23], $\eta(\mathbf{r}) \equiv \frac{\Delta n(\mathbf{r})}{n(\mathbf{r})} = \frac{8}{3\sqrt{\pi}} \sqrt{n(\mathbf{r})a^3} F_D(\epsilon_{dd})$, with $F_D(\epsilon_{dd}) = \frac{1}{2} \int d\theta_k \sin\theta_k f(\epsilon_{dd},\theta_k)^{3/2}$. In our simulations, $\eta(\mathbf{r}) \lesssim 0.01$ at any point and time.

We consider a BEC with N Dy atoms, with $|\mu| = 10\mu_B$, with μ_B the Bohr magneton. In order to compare our results with recent experiments [14] we assume $\omega_{x,y,z}/2\pi = (44,46,133)$ Hz (droplets may form in other trap geometries as well, but the details of the stability threshold, as well as of the droplet nucleation, vary with the precise trap). We employ an imaginary-time evolution of Eq. (3) to form an initial BEC with $a = 120a_B$, with a_B the Bohr radius. Under these conditions, the BEC, with a wave function $\psi_0(\mathbf{r})$, is stable and in the TF regime. At finite temperature T , thermal fluctuations seed the modulational instability after the quench of a discussed below, and may influence droplet nucleation. Following Ref. [18], we add thermal fluctuations (for $T = 20$ nK) in the form $\psi(\mathbf{r},t=0) = \psi_0(\mathbf{r}) + \sum_n \alpha_n \phi_n$, where ϕ_n are eigenmodes of the harmonic trap with eigenenergies ϵ_n , the sum is restricted to $\epsilon_n < 2k_B T$, and α_n is a complex Gaussian random variable with $\langle |\alpha_n|^2 \rangle = \frac{1}{2} + (e^{\epsilon_n/k_B T} - 1)^{-1}$. Similar results are obtained using a stochastic Gross-Pitaevskii equation to create the thermal excitations.

At $t = 0$ we quench in 0.5 ms to a final $a = 70a_B$ that destabilizes the BEC. This value is chosen to ensure that even small condensates are destabilized as the threshold depends on the number of particles and quenches to $a = 80a_B$ destabilize only condensates with $N \gtrsim 10000$. The most unstable Bogoliubov mode has a nonzero angular momentum. As a result, the BEC develops at $T = 0$ an initial ringlike modulational instability on the xy plane, followed by azimuthal symmetry breaking into droplets. At finite T , droplets may nucleate from thermal fluctuations before the ring develops (as experimentally observed [25]). In both cases stable droplets form in a few ms, which arrange in a quasicrystalline structure (Fig. 1), in excellent agreement with Ref. [14]. Droplet nucleation does not involve, however, the whole condensate. A significant number of atoms remain in a halolike background too dilute to gather particles into stable droplets (approximately 30% in Fig. 1, barely visible due to the contrast).

Stable droplets result from the compensation at large-enough densities of the attractive MF term $\mu_0 \propto n(\mathbf{r})$ by the effective repulsion introduced by the LHY term $\Delta\mu \propto n(\mathbf{r})^{3/2}$. Note that, as mentioned above, this occurs even for very low condensate depletion because the MF term μ_0 is characterized already by an almost complete cancellation of the short-range and dipolar contributions. In order to study the properties of individual droplets, we evolve Eq. (3) in imaginary time for $a = 70a_B$. In order to guarantee the formation of a single droplet in our numerics, we employ as an initial condition

for the imaginary-time evolution an elongated Gaussian wave function at the trap center very compressed on the xy plane. Using other initial conditions, in particular, a pancake wave function elongated on the xy plane, results in the formation of variable droplet configurations similar to those discussed below in the real-time evolution. In passing, this shows that droplet nucleation and the formation of (metastable) droplet structures should occur not only in the postquench dynamics, but also when directly forming the condensates at sufficiently low scattering lengths, as discussed in Ref. [14].

Figure 2 shows the droplet energy per particle E_D (including the LHY correction) as a function of the number of particles in the droplet N_D . Two important features are worth mentioning. There is a minimal particle number, $N_{\min} \simeq 900$, such that for $N_D < N_{\min}$ no stable droplet may form. If the local density does not allow for the gathering of that critical number, then no droplet is formed, accounting for the background halo. Second, $E_D(N_D)$ presents a nonmonotonous dependence with N , showing a minimum (at $N_D \simeq 13\,000$ in Fig. 2), being only positive at N_D values close to N_{\min} ($E_D = 0$ at $N_D \simeq 1500$ in Fig. 2). This is particularly relevant for droplet nucleation in quench experiments. The BEC energy, which after the quench is initially positive ($\simeq 8\hbar\tilde{\omega}$ in Fig. 1), is almost conserved during the droplet formation, just decreasing in a much longer-time scale due to 3BLs. The final droplet gas is characterized by the internal energy of the droplets, the center-of-mass (c.m.) energy of the droplets, and the interdroplet repulsive DDIs (the much more dilute halo has a comparatively small contribution). Although the c.m. energy and the repulsive interdroplet interaction are obviously positive, they cannot balance a negative internal energy of the droplets, as required by the quasiconservation of the energy mentioned above. This explains why, as shown below, in quench experiments droplets form with particle numbers between 900 and 1500, despite the fact that bigger droplets could be stable (Fig. 2).

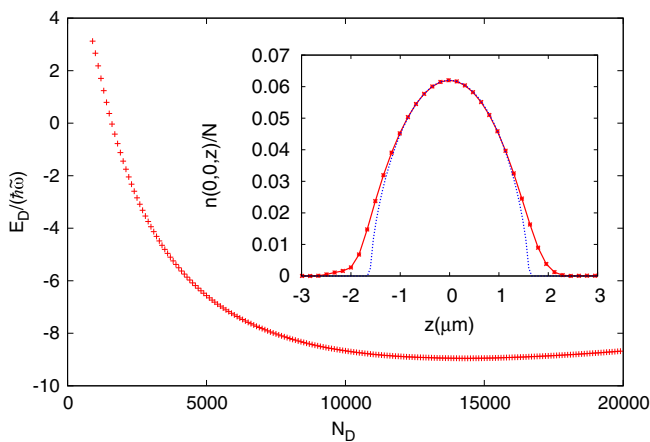


FIG. 2. Droplet energy per particle E_D [in units of $\hbar\tilde{\omega}$, with $\tilde{\omega} = (\omega_x\omega_y\omega_z)^{1/3}$] as a function of the number of particles in the droplet N_D for $a = 70a_B$; for $N_D < N_{\min} \simeq 900$ no stable droplet is found. Droplets with $E_D > 0$ occur for $N_D \lesssim 1500$. In the inset, we show the density profile (solid line with crosses) of a droplet with $N_D = 1000$ at the trap center for the cut $x = y = 0$. At the droplet center, $n(0,0,z) \propto (1 - z^2/Z^2)^{2/3}$ (dotted curve).

The droplets are markedly elongated along z . For $N_D \simeq 1000$, the z half size is $\simeq 2\ \mu\text{m}$, whereas along xy is $\lesssim 0.3\ \mu\text{m}$. This elongation is required for the attractive DDIs to overwhelm the repulsive contact MF term. The droplets are in any case in the TF regime along z . Note that due to the LHY term, the droplets do not present an inverted-paraboloid profile even in the TF regime, but rather $n(x = 0, y = 0, z) \sim (1 - z^2/Z^2)^{2/3}$ (inset of Fig. 2). Droplets with $N_D > 8000$ are also TF along xy , whereas those with $N_D < 4000$ are approximately Gaussian. The latter is also the case for the droplets, discussed below, that are formed in real time after a quench. Quantum pressure is hence non-negligible for small droplets, but it is not crucial for the droplet stability, which is provided by the compensation of the attractive MF interaction and the LHY correction. This is in stark contrast with bright solitons, which result from the compensation of quantum pressure and attractive interactions [26,27].

We return at this point to the droplet nucleation in quench experiments. We have performed for different N simulations of the BEC dynamics after the quench of a , starting from different initial conditions given by random thermal fluctuations. As in the experiments, we observe that the droplets arrange in crystal-like patterns (see Fig. 1), although they present a residual dynamics. The number of particles in a droplet varies from droplet to droplet in a single realization and between realizations (as in the actual experiments) since stable droplets may be formed for different $N_D > N_{\min}$. The variance of the number of droplets is additionally affected by the variable importance of the background halo. In addition, droplets formed at the verge of instability, $N_D \simeq N_{\min}$, may become unstable against melting in the halo, and hence the droplet number may vary in time. In order to determine objectively the droplet number, we have obtained the column density, $n_{XY}(x, y) \equiv \int dz n(\mathbf{r})$, after 20 ms of postinstability dynamics, and defined a droplet as such if it reaches a maximal $n_{X,Y}/N > 0.3$ (see, e.g., Fig. 1). Figure 3(a) summarizes our results. The droplet number shows an approximate linear dependence with N , in agreement with experiments. The deviation at larger N occurs because at 20 ms there are droplets about to be nucleated in the outer halo regions but not fully formed (according to the previous criterion). The deviation at low N is due to the longer time needed to develop droplets (e.g., $N = 5000$ develops up to three droplets at $t \sim 40$ ms). The approximate linear dependence of Fig. 3(a) stems from the local character of the nucleation, which results in a particle number per droplet basically independent of N [inset of Fig. 3(a)]. The histogram of Fig. 3(b) shows that, as expected from our discussion of the droplet energy, the particle number per droplet lies between 900 and 1500, with an average of approximately 1200, again in good agreement with experiments.

We obtain peak densities of $\sim 2 \times 10^{21}\ \text{m}^{-3}$ [28]. At those densities 3BLs become relevant in the long run. We take them into account by adding the term $-i\frac{\hbar L_3}{2} |\psi(\mathbf{r})|^4 \psi(\mathbf{r})$ [13] to the right-hand side of Eq. (3), with $L_3 = 1.2 \times 10^{-41}\ \text{m}^6/\text{s}$ [29]. Figure 4 shows the time dependence of the atom number and of the spectral weight, $\text{SW} = \int d^2k \tilde{n}_{XY}(\mathbf{k})$, where $\tilde{n}_{XY}(\mathbf{k})$ is the Fourier transform of $n_{XY}(x, y)$ and the integral extends from $k_{\min} = 1.5\ \mu\text{m}^{-1}$ to $k_{\max} = 5\ \mu\text{m}^{-1}$. The spectral weight

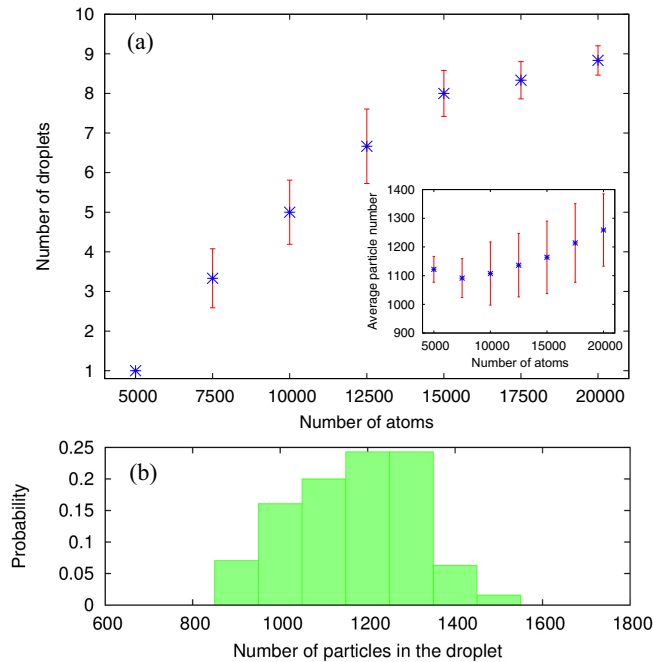


FIG. 3. (a) Droplet number as a function of the initial atom number N , 20 ms after a quench from $a = 120a_B$ to $70a_B$. Inset: Atom number per droplet as a function of N under the same conditions. In both cases the average is denoted by a blue cross, and the variance by the error bar. (b) Histogram of the atom number per droplet for the same conditions evaluated from a sample of 260 droplets.

characterizes the appearance (and disappearance) of the droplet pattern [14]. The losses not only decrease the atom number, but also lead to the destruction of droplets, which may lose too many particles to remain stable against melting in the background. Moreover, the slow energy dissipation induced by 3BLs at the BEC maxima is relevant for the formation of droplet arrangements (Fig. 1) that minimize interdroplet repulsion. Figure 4 shows a growth of SW up to $t \sim 10$ ms, and a decrease in a much longer-time scale of several hundreds of ms, accompanied by the corresponding atom loss, in excellent agreement with experiments.

In summary, quantum fluctuations prevent collapse in unstable dipolar BECs, leading to droplet formation, accounting for recent Dy experiments. Since the LHY correction depends on na^3 , we expect that droplets should collapse for lower a , providing a criterion to discern LHY stabilization from stabilization based on three-body forces [17,18]. Our results,

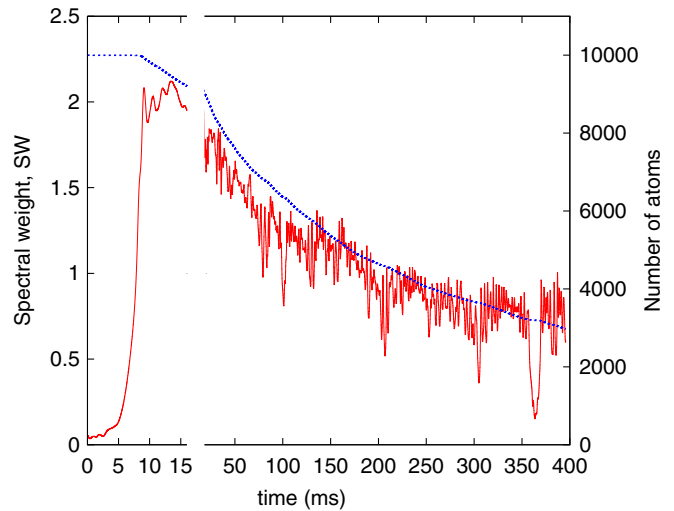


FIG. 4. Atom number (blue dotted) and spectral weight (red solid) as a function of the time after a quench from $a = 120a_B$ to $70a_B$ for a BEC with initially 10 000 atoms.

based on a generalized NLNLSE, are already in very good agreement with experiments [14,19], although a more precise analysis of long-wavelength excitations in small droplets may be necessary to provide a fully quantitative comparison, in particular, in what concerns the peak density in the droplets. We stress that LHY stabilization results from the anisotropy of the DDIs. It was absent in chromium experiments [13] because the BEC became unstable at $a \simeq 10$ times smaller than in Dy [30]. Quantum stabilization would have hence demanded in chromium densities at least 10^3 times larger than in Dy ($n > 10^{24} \text{ m}^{-3}$), due to the na^3 dependence of the LHY term. These densities are, however, unreachable due to 3BLs. In contrast, LHY stabilization and droplet nucleation are a characteristic general feature induced by the DDIs that should play a key role in all future experiments with strongly dipolar gases of highly magnetic atoms and polar molecules.

Note added. Recent results based on path-integral Monte Carlo calculations [31] have confirmed the validity of the generalized NLNLSE approach for the description of the quantum droplets discussed in our Rapid Communication.

We thank D. Petrov and Y. Li for comments, and H. Kadau, I. Ferrier-Barbut, and T. Pfau for insightful exchanges and for sharing their experimental results. We acknowledge support by the center QUEST, and the DFG Research Training Group 1729.

- [1] See, e.g., T. Lahaye, C. Menotti, L. Santos, M. Lewenstein, and T. Pfau, *Rep. Prog. Phys.* **72**, 126401 (2009), and references therein.
- [2] See, e.g., M. A. Baranov, M. Dalmonte, G. Pupillo, and P. Zoller, *Chem. Rev.* **112**, 5012 (2012), and references therein.
- [3] A. Griesmaier, J. Werner, S. Hensler, J. Stuhler, and T. Pfau, *Phys. Rev. Lett.* **94**, 160401 (2005).

- [4] M. Lu, N. Q. Burdick, S. H. Youn, and B. L. Lev, *Phys. Rev. Lett.* **107**, 190401 (2011).
- [5] K. Aikawa, A. Frisch, M. Mark, S. Baier, A. Rietzler, R. Grimm, and F. Ferlaino, *Phys. Rev. Lett.* **108**, 210401 (2012).
- [6] A. de Paz, A. Sharma, A. Chotia, E. Maréchal, J. H. Huckans, P. Pedri, L. Santos, O. Gorceix, L. Vernac, and B. Laburthe-Tolra, *Phys. Rev. Lett.* **111**, 185305 (2013).

- [7] K.-K. Ni, S. Ospelkaus, M. H. G. de Miranda, A. Pe'er, B. Neyenhuis, J. J. Zirbel, S. Kotochigova, P. S. Julienne, D. S. Jin, and J. Ye, *Science* **322**, 231 (2008).
- [8] B. Yan, S. A. Moses, B. Gadway, J. P. Covey, K. R. A. Hazzard, A. M. Rey, D. S. Jin, and J. Ye, *Nature (London)* **501**, 521 (2013).
- [9] T. Takekoshi, L. Reichsöllner, A. Schindewolf, J. M. Hutson, C. R. Le Sueur, O. Dulieu, F. Ferlaino, R. Grimm, and H.-C. Nägerl, *Phys. Rev. Lett.* **113**, 205301 (2014).
- [10] J. W. Park, S. A. Will, and M. W. Zwierlein, *Phys. Rev. Lett.* **114**, 205302 (2015).
- [11] See, e.g., J. B. Balewski, A. T. Krupp, A. Gaj, S. Hofferberth, R. Löw, and T. Pfau, *New J. Phys.* **16**, 063012 (2014).
- [12] T. Koch, T. Lahaye, J. Metz, B. Fröhlich, A. Griesmaier, and T. Pfau, *Nat. Phys.* **4**, 218 (2008).
- [13] T. Lahaye, J. Metz, B. Fröhlich, T. Koch, M. Meister, A. Griesmaier, T. Pfau, H. Saito, Y. Kawaguchi, and M. Ueda, *Phys. Rev. Lett.* **101**, 080401 (2008).
- [14] H. Kadau, M. Schmitt, M. Wenzel, C. Wink, T. Maier, I. Ferrier-Barbut, and T. Pfau, *Nature (London)* **530**, 194 (2016).
- [15] M. D. Cowley and R. E. Rosensweig, *J. Fluid Mech.* **30**, 671 (1967).
- [16] J. V. I. Timonen, M. Latikka, L. Leibler, R. H. A. Ras, and O. Ikkala, *Science* **341**, 253 (2013).
- [17] K.-T. Xi and H. Saito, *Phys. Rev. A* **93**, 011604(R) (2016).
- [18] R. N. Bisset and P. B. Blakie, *Phys. Rev. A* **92**, 061603(R) (2015).
- [19] I. Ferrier-Barbut, H. Kadau, M. Schmitt, M. Wenzel, and T. Pfau, *Phys. Rev. Lett.* **116**, 215301 (2016).
- [20] D. S. Petrov, *Phys. Rev. Lett.* **115**, 155302 (2015).
- [21] R. Schützhold, M. Uhlmann, Y. Xu, and U. R. Fischer, *Int. J. Mod. Phys. B* **20**, 3555 (2006).
- [22] A. R. P. Lima and A. Pelster, *Phys. Rev. A* **84**, 041604(R) (2011).
- [23] A. R. P. Lima and A. Pelster, *Phys. Rev. A* **86**, 063609 (2012).
- [24] S. Ronen, D. C. E. Bortolotti, and J. L. Bohn, *Phys. Rev. A* **74**, 013623 (2006).
- [25] H. Kadau and T. Pfau (private communication).
- [26] L. Khaykovich, F. Schreck, G. Ferrari, T. Bourdel, J. Cubizolles, L. D. Carr, Y. Castin, and C. Salomon, *Science* **296**, 1290 (2002).
- [27] K. E. Strecker, G. B. Partridge, A. G. Truscott, and R. G. Hulet, *Nature (London)* **417**, 150 (2002).
- [28] These densities are larger than those in recent experiments [19] by a factor of 3–4. Note that the LHY corrections depend on na^3 and hence a larger a may reduce the density. Even more relevantly, the prefactor of the LHY term may be modified for small droplets by short-wavelength excitations. An increase in the prefactor will further decrease the peak density.
- [29] The exact value of L_3 is not yet known but it should be in the lower 10^{-41} m⁶/s. See M. Lu, Quantum Bose and Fermi gases of dysprosium: production and initial study, Ph.D. thesis, Stanford University, 2014.
- [30] For Dy, $m|\mu|^2$ is 10 times larger than in Cr.
- [31] H. Saito, *J. Phys. Soc. Jpn.* **85**, 053001 (2016).